



# Characterisation of dust aerosols from ALADIN and CALIOP measurements

Rui Song<sup>1</sup>, Adam Povey<sup>1,2</sup>, and Roy G. Grainger<sup>1</sup>

<sup>1</sup>National Center for Earth Observation, Atmospheric, Oceanic and Planetary Physics, University of Oxford, Oxford, OX1 3PU, UK

<sup>2</sup>Now at National Center for Earth Observation, Physics and Astronomy, University of Leicester, Leicester, LE4 5SP, UK

**Correspondence:** Rui Song (rui.song@physics.ox.ac.uk)

**Abstract.** Atmospheric aerosols have a pronounced effect on climate dynamics at both regional and global scales, but the magnitude of these effects is subject to considerable uncertainties. A major contributor to these uncertainties is the incomplete understanding of aerosol's vertical structure, largely due to observational limitations. Spaceborne lidars can directly observe the vertical distribution of aerosols globally, and are increasingly used in atmospheric aerosol remote sensing. As the first spaceborne High Spectral Resolution Lidar (HSRL), the ALADIN instrument onboard the Aeolus satellite was operational from 5 2018 to 2023. With its sophisticated design, ALADIN can retrieve aerosol backscatter and extinction coefficients separately without an assumption of the lidar ratio. This study is dedicated to assessing the performance of ALADIN's aerosol retrieval capabilities by comparing them with CALIOP measurements. A statistical analysis of retrievals from both instruments during the June 2020 Saharan dust event indicates good consistency between the observed backscatter and extinction coefficients. A 10 detailed comparison of extinction coefficients for dust layers reveals that ALADIN is more susceptible to signal attenuation than CALIOP. During this extreme dust event, CALIOP-derived aerosol optical depth (AOD) exhibited large discrepancies with MODIS Aqua measurements. Using collocated ALADIN observations to revise the dust lidar ratio to 63.5 sr, AODs retrieved from CALIOP are increased by 46%, improving the comparison with MODIS data. Further, the combination of measurements from ALADIN and CALIOP can enhance the tracking of aerosols' vertical transport. This study demonstrates the potential for 15 spaceborne HSRL to retrieve aerosol optical properties. It highlights the benefits of spaceborne HSRL in directly obtaining the lidar ratio, significantly reducing uncertainties in extinction retrievals. This work paves the way for forthcoming spaceborne HSRL missions, particularly the ESA ATLID space lidar (set for a 2024 launch) and Aeolus-2.

## 1 Introduction

Atmospheric aerosols have a pronounced effect on climate dynamics at both regional and global scales. They directly affect 20 the climate by scattering and absorbing both shortwave and longwave radiation (Ghan et al., 2012; Myhre et al., 2013; Oikawa et al., 2018). Aerosols also have an indirect effect through their interactions with clouds by modifying their microphysical characteristics, radiative properties, and lifetime (Altaratz et al., 2014; Bellouin et al., 2020). Such interactions alter the net radiation fluxes at the top of the atmosphere and the surface. The magnitude of these effects is subject to considerable uncertainties. These uncertainties are attributed to limitations in the description of aerosol properties, the spatio-temporal variation of



25 aerosols, and particularly, inadequate understanding of the vertical structures of aerosols. The vertical distribution of aerosols is driven by atmospheric transport patterns, residence times, and the efficiency of vertical transport (Koffi et al., 2012) which vary by up to an order of magnitude among models (Textor et al., 2006; Kipling et al., 2016). Minimising the considerable uncertainties in aerosol vertical distributions is crucial for accurately assessing the effects of aerosols on the climate system.

Vertical dispersal patterns of aerosols have become better constrained since the development of lidar technology. Ground-based lidar networks, such as the European Aerosol Research lidar NETwork (EARLINET) (Pappalardo et al., 2014), the Micro Pulse lidar NETwork (MPLNET) (Welton et al., 2001), and the Asian Dust and Aerosol lidar Observation NETwork (AD-Net) (Sugimoto et al., 2016), provide detailed vertical aerosol profiles on regional scales.

The limitation in spatial coverage of ground lidar was partially overcome with the launch of lidar into orbit. Spaceborne lidars have the advantage of minimal aerosol loading between the instrument and the calibration region. Lidars launched into orbit include the Lidar In-Space Technology Experiment (LITE) (Winker et al., 1996), the Geoscience Laser Altimeter System (GLAS) (Spinhirne et al., 2005), the Cloud-Aerosol Transport System (CATS) (McGill et al., 2015), and the Advanced Topographic Laser Altimeter System (ATLAS) (Markus et al., 2017). The Cloud-Aerosol Lidar with Orthogonal Polarization (CALIOP) (Winker et al., 2010) instrument onboard the Cloud-Aerosol Lidar and Infrared Pathfinder Satellite Observations (CALIPSO) satellite, launched in 2006, was tailored to offer vertical profile measurements of both clouds and aerosols coincident with other observations in NASA's A-Train. CALIOP emits laser pulses toward the Earth's surface, capturing attenuated backscattered signals at 532 and 1064 nm from which the profile of aerosol backscatter and extinction coefficients can be retrieved. CALIOP measures the linear depolarization of the backscattered signals, facilitating the discrimination of cloud phase and identification of non-spherical aerosols (such as mineral dust, volcanic ash, and soot). The Atmospheric Laser Doppler Instrument (ALADIN) (Stoffelen et al., 2005) onboard the European Space Agency's Aeolus mission further advanced this field by launching a HSRL. Operational from 2018 until 2023, ALADIN was a state-of-the-art Direct Detection Doppler Wind lidar that operated at 355 nm. While its primary focus was detecting wind patterns, this study considers aerosol backscatter and extinction coefficient retrievals from ALADIN and compares them with CALIOP retrievals.

As an elastic backscatter lidar, CALIOP needs the particle extinction-to-backscatter ratio, commonly referred to as the lidar ratio, to accurately interpret the signals. While its value depends on the microphysical characteristics of aerosols, including their refractive index and size distribution, lidar ratio is unaffected by aerosol concentration (Mona et al., 2006). The lidar ratio enables the derivation of particle extinction coefficients from single-channel backscatter profiles, and is therefore fundamental to accurate estimation of aerosol radiative impact. However, there remain limitations in CALIOP's lidar ratio selection scheme. For example, the use of a single lidar ratio for all dust aerosols introduces bias (Kim et al., 2020) because the lidar ratio is influenced by the mineralogical composition and refractive index of dust particles (Schuster et al., 2012) and particle nonsphericity (Dubovik et al., 2006). Beyond the limitations associated with selecting a constant lidar ratio for specific aerosol types, CALIOP's extinction retrieval presents additional challenges. There is a minimum AOD detectable by CALIOP, which affects how observations should be compared (Watson-Parris et al., 2018), with the undetected layers having a global mean AOD of  $0.031 \pm 0.052$  (Kim et al., 2017).



High Spectral Resolution Lidars (HSRLs) are increasingly recognised for their potential in atmospheric aerosol remote sensing as they separately detect particles and molecules (Shiple et al., 1983; Müller et al., 2014; Wang et al., 2022). A significant advantage of this technique is that the aerosol retrieval is independent of assumptions regarding the lidar ratio. The aerosol and cloud retrievals from ALADIN have been systematically validated against a variety of ground-based measurements (Baars et al., 2021; Paschou et al., 2022; Abril-Gago et al., 2022; Feofilov et al., 2022; Gkikas et al., 2023). The ALADIN instrument employs a circularly polarized emission, but only detects the co-polar component of the return. Due to this instrument configuration, ALADIN's aerosol retrieval underestimates the aerosol backscatter coefficient for highly depolarized atmospheric particles (Paschou et al., 2022; Gkikas et al., 2023), including ice crystals, smoke, dust, and volcanic ash. However, this mis-detection of cross-polar component backscattered signals does not influence the retrieval of the extinction coefficient. The aerosol processing in ALADIN does not rely on the information of the lidar ratio. Instead, ALADIN is capable of retrieving the lidar ratio as a variable within its Level-2 aerosol products. However, given that its aerosol retrieval process does not set constraints on the lidar ratio, the retrieved lidar ratio often exhibits significant fluctuations for a given aerosol layer. One scenario leading to this variability is when the backscattered signal approaches the instrument's detection threshold. Thus, effective filtering is essential when analysing ALADIN lidar ratios. Additionally, ALADIN's Level-2 backscatter and extinction coefficients are subject to independent Quality Control (QC) procedures. Despite these challenges, it has been demonstrated that ALADIN is capable of retrieving lidar ratios from smoke (Baars et al., 2021), dust (Flament et al., 2021) and marine aerosols (Sun et al., 2023).

This study aims to explore and demonstrate the capabilities of ALADIN in retrieving aerosol optical properties, specifically the backscatter coefficient, extinction coefficient, and lidar ratio. The CALIOP Level-2 aerosol products, with a 5-km horizontal resolution, are used as a benchmark. The Saharan dust in June 2020 is chosen as the study area. Firstly, desert dust is the most predominant aerosol by mass in the atmosphere. Secondly, the lidar ratio of dust exhibits pronounced geographic variations. Finally, the Saharan dust event of June 2020 serves as a unique challenge, acting much like a stress test for evaluating space lidar measurements (particularly where the dust layer can fully attenuate the return). In this study, a statistical analysis was undertaken to compare ALADIN and CALIOP in their retrieval of aerosol backscatter and extinction coefficients. To further understand the underlying causes of discrepancies in extinction retrievals, a comparison was made between the dust lidar ratio values assumed by CALIOP and those retrieved by ALADIN. This paper also introduces findings from the combined utilisation of both spaceborne lidars to trace the vertical transport of a dust plume within a specified region.

This paper is structured as follows. Section 2 introduces the aerosol products of Aeolus-ALADIN and CALIPSO-CALIOP and analyses the collocation between these two spaceborne lidars. Section 3 highlights the challenges of differentiating between aerosol and cloud in ALADIN data and proposes a solution by using a dust mask derived from coincident geostationary satellite observations. Section 4 compares the retrieval of aerosol backscatter and extinction coefficients from ALADIN and CALIOP, focusing on the Saharan dust event of June 2020. Section 5 provides an in-depth analysis of extinction retrievals at different altitude layers, utilising collocated measurements from both lidar systems. Section 6 further explores the dust lidar ratio, a key parameter influencing the observed discrepancies in extinction retrievals, and evaluates these findings by comparing the



AOD with MODIS measurements. Section 7 is dedicated to demonstrating the potential of combining ALADIN and CALIOP measurements in enhancing the tracking of aerosol vertical movement. Finally, Section 8 concludes this paper.

## 95 2 Data

This section introduces the aerosol products from Aeolus-ALADIN and CALIPSO-CALIOP, followed by a discussion of the collocations between the two instruments.

### 2.1 Aeolus-ALADIN aerosol products

Aeolus was launched into space on 22 August 2018 and concluded its mission on 30 April 2023, operating in a Sun-synchronous orbit at an altitude of 320 km with an inclination angle of  $97^\circ$ . The Aeolus satellite hosted ALADIN as its sole payload, which was equipped with an Nd:YAG laser, emitting narrow-bandwidth UV laser pulses at a wavelength of 355 nm. Completing 16 orbits per day, Aeolus maintained a revisit time of 7 days. The laser was directed at an off-nadir angle of  $35^\circ$  as the primary mission was the sounding of horizontal winds.

Each observation by ALADIN integrates laser shots over a 12-second interval, corresponding to an along-track horizontal resolution of approximately 87 km. Each observation is comprised of 24 vertical bins, with varying vertical resolutions: 0.5 km between 0 and 2 km, 1 km between 2 and 16 km, and 2 km between 16 and 30 km. This spacing was adjustable to meet the requirements of specific scenarios. For instance, the ceiling was increased to 30 km near the Hunga Tonga–Hunga Ha’apai plume ( $30^\circ$  S -  $0^\circ$ ) in response to the changes observed a few days after the eruption on 15 January 2022 (Legras et al., 2022).

The ALADIN Level-2A products are derived using several algorithms, including the Standard Correction Algorithm (SCA), Standard Correction Algorithm middle bin (SCAmb), and the Maximum-Likelihood Estimation (MLE) (Ehlers et al., 2022). The SCA aerosol retrieval is an algebraic inversion scheme that relies on processing cross-talk-corrected signals from both the Rayleigh and Mie channels (Flament et al., 2021). An assessment over the eastern Mediterranean demonstrated that the SCA backscatter coefficients were in good agreement with ground measurements for horizontally homogeneous, fine spherical particles at altitudes below 4 km. However, the performance of the SCA degrades in the lowermost bins, attributed to either contamination from surface signals or to increased noise levels (Gkikas et al., 2023). Another limitation of the SCA method is that the errors in extinction propagate from the first (uppermost) bin to underlying bins. To address this limitation, the SCAmb method averages extinction values over two consecutive bins. Although this results in a reduction in vertical resolution, the trade-off leads to a significant improvement quality. By adapting the SCA method into a physically constrained optimal estimation framework, the MLE method demonstrates a predominantly positive impact coupled with considerable noise suppression. The enhancements effected by the MLE method largely arise from the imposition of positivity constraints on optical properties and the employment of a bounded lidar ratio (Ehlers et al., 2022). In this work, the Level-2 SCAmb products are used to examine ALADIN’s aerosol retrieval performance.

## 2.2 CALIPSO-CALIOP aerosol products

The CALIPSO satellite, with the CALIOP instrument as its primary payload, was launched in 2006 alongside CloudSat, subsequently joining the A-Train (afternoon constellation). It is approximately 73 seconds behind the MODIS Aqua satellite. This orbital configuration guarantees frequent collocations between CALIOP and MODIS measurements. The specifics of this collocation process are detailed in Kim et al. (2017), where the collocated MODIS AOD serves as an additional constraint on CALIOP extinction retrievals. Due to technical challenges affecting its maneuvering capability, CloudSat exited the A-Train to a lower orbit in February 2018. By September of the same year, CALIPSO rejoined CloudSat in what is now called as the C-Train. This orbit is 16.5 km below the A-Train, resulting in a slightly different ground track.

CALIOP Level-2 products include the physical and optical parameters associated with detected aerosol and cloud layers. The utilisation of the Iterated Boundary Location (SIBYL) algorithm aims to optimise the detection of weakly scattering layers while maintaining reliable identification of dense layers. Nonetheless, given that SIBYL operates based on a threshold-based detection mechanism, it may occasionally overlook optically thin features that fall below the detection threshold. Subsequent to detection, the aerosol layers undergo classification into distinct aerosol types. This classification is identified by the Scene Classification Algorithm (Kim et al., 2018), a decision-tree based method that takes into account factors such as altitude, geographical location, surface type, estimated particulate depolarization ratio, and integrated attenuated backscatter. In the final phase, the Level-2 extinction coefficient is retrieved from the Hybrid Extinction Retrieval Algorithm (HERA) (Winker et al., 2010; Young et al., 2018). The CALIOP Level 1 data provides a horizontal resolution of 333 m and a variable vertical resolution: 30 m below 8 km and 60 m in the range of 8 to 20 km. In contrast, the CALIOP Level 2 aerosol products present a horizontal resolution of 5 km. The vertical resolution is 60 m up to an altitude of 20.2 km and transitions to 180 m between 20.2 km and 30.1 km.

In the CALIOP Level-2 Scene Classification V3 and earlier versions, aerosols are categorised into six distinct categories: clean marine, dust, polluted continental, clean continental, polluted dust, and smoke (Omar et al., 2009). Each aerosol category is assigned a specific lidar ratio, along with a corresponding uncertainty value. That scheme tended to misclassify aerosols in regions with a mixture of different aerosol types (Burton et al., 2012; Nowottnick et al., 2015), and it lacks a mechanism for identifying stratospheric aerosol types. Such aerosol misclassifications can lead to 30-50% uncertainty in the selected lidar ratio, introducing bias in CALIOP's retrievals (Rogers et al., 2014; Amiridis et al., 2013; Burton et al., 2013). To address these shortcomings, the CALIOP V4 Scene Classification Algorithm enhanced aerosol subtyping, expanding the number of aerosol types to 11, covering both tropospheric and stratospheric aerosols (Kim et al., 2018). V4 also revised the lidar ratios designated for different aerosol subtypes. Owing to these enhancements, CALIOP V4 demonstrates reduced bias in AOD when compared to AERONET and Moderate Resolution Imaging Spectroradiometer (MODIS) measurements. In this study, the CALIOP Level-2 V-4.21 aerosol profiles (*CAL\_LID\_L2\_05kmAPro-Standard-V4-21\_V4-21*) are used for comparison against ALADIN aerosol retrievals.

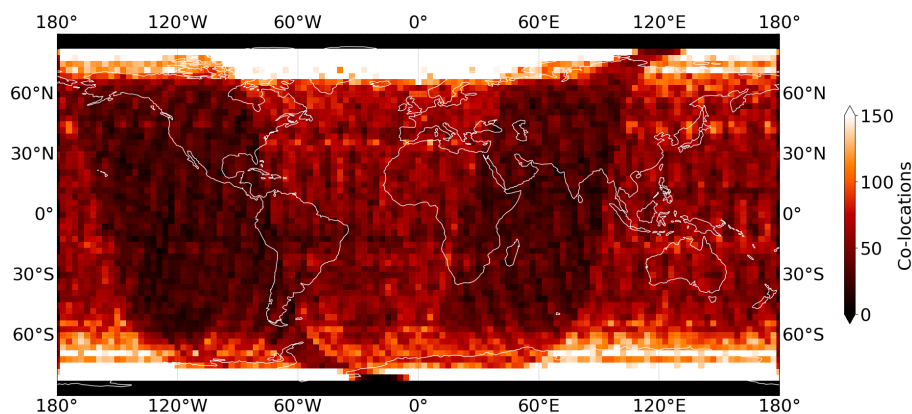


**Figure 1.** Global distribution of collocated ALADIN and CALIOP profiles from 30<sup>th</sup> June 2019 to 28<sup>th</sup> September 2021. The plot, based on a  $3^\circ \times 3^\circ$  grid, sets the maximum temporal disparity at 9 hours and the maximum spatial difference at 200 km.

### 155 2.3 Collocation of Aeolus and CALIPSO

Aeolus performs its overpass of the equator at 06:00 and 18:00 LST, whereas CALIPSO does so at 01:30 and 13:30 LST. The ALADIN lidar has a line-of-sight that is  $35^\circ$  off-nadir towards the Earth's night side. In contrast, the CALIPSO lidar probes the Earth's atmosphere from a nearly nadir angle of  $3^\circ$ . Collocation between Aeolus and CALIPSO represents a balance between the quantity of collocated profiles and their coincidence. In their examination of the scattering ratio profiles from both ALADIN and CALIOP, Feofilov et al. (2022) highlighted the collocation between the two space lidars. They established a collocated database with a spatial distance under  $1^\circ$  and a temporal discrepancy not exceeding 24 hours, based on data between 30<sup>th</sup> June 160 and 28<sup>th</sup> September 2021. Fig. 1 is a representation of the global distribution of these collocated profiles.

In Fig. 1, it is evident that collocations are concentrated at the poles. The distribution of temporal disparity and spatial distance between collocations, for three latitude bands, are shown in Fig. 2. Between  $30^\circ$  N and  $30^\circ$  S, most collocated 165 observations are within 4 hours and 100 km.

### 3 Aerosol and cloud discrimination

CALIOP's effectiveness in distinguishing between various aerosols and clouds can be largely attributed to its measurements of particle depolarization ratio at 532 nm and its colour ratio between 532 and 1064 nm. With version 4.5 (Tackett et al., 2023), enhancements were made to the CALIOP Level-2 aerosol products, primarily focusing on the improved accuracy of 170 stratospheric aerosol classification.

ALADIN, limited by its single-band observation and its inability to capture particle depolarization information, faces a significant challenge when it comes to discriminating between aerosols and clouds. van Zadelhoff et al. (2023) developed a method known as the ATLID FeatureMask (A-FM) for detecting aerosol and cloud features, intended for use with the forth-

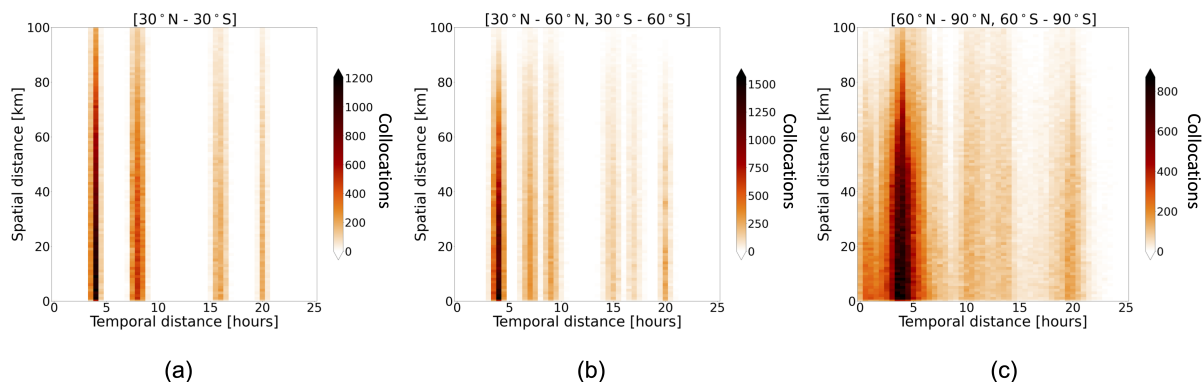


**Figure 2.** Temporal disparity and spatial distance of collocated ALADIN and CALIOP profiles at (a) 30° N - 30° S, (b) 30° N - 60° N and 30° S - 60° S, (c) (b) 60° N - 90° N and 60° S - 90° S.

coming high spectral resolution UV lidar (ATLID) onboard the EarthCARE satellite mission. Initially, the A-FM method was  
 175 evaluated using synthetic data from the EarthCARE end-to-end simulator (ECSIM) and real observations from ALADIN's  
 L1 data. It was then adapted into the operational Aeolus FeatureMask (AEL-FM), which is now included in the official L2A  
 Aeolus processor. Another aerosol and cloud discrimination method is proposed in Flament et al. (2021). This method utilises  
 auxiliary meteorological information provided by the European Centre for Medium-Range Weather Forecasts (ECMWF) to  
 identify cloud-free conditions. Both aerosol and cloud discrimination methods highlighted above have undergone updates,  
 180 enhancing their accuracy in aerosol and cloud typing. The discrimination methods are planned to be applied during the repro-  
 cessing of the ALADIN aerosol products, and both cloud masks will be incorporated into the future releases of ALADIN L2A  
 products.

At the time of this paper's writing, the ALADIN L2A data from the study period does not include the advanced cloud masks  
 described, prompting the exploration of alternatives. In the assessment of Aeolus particle backscatter coefficient retrievals in  
 185 the eastern Mediterranean, Gkikas et al. (2023) used the cloud mask product obtained from the Spinning Enhanced Visible and  
 Infrared Imager (SEVIRI) instrument mounted on the Meteosat Second Generation (MSG) geostationary satellite (Schmetz  
 et al., 2002). This cloud mask was used to filter out cloud-contaminated data from ALADIN L2A aerosol products, proving to  
 be an effective approach. This work is focused on the East Atlantic region, which frequently experiences the transport of dense  
 dust plumes from the Sahara. In this context, differentiating between thick dust and clouds using the SEVIRI cloud mask has  
 190 proven challenging. As a result, rather than employing a standard cloud mask to filter out cloud-contaminated data for space  
 lidar observations, this study uses a dust mask to identify lidar observations that capture only dust plumes.

Figure 3 provides a comparison of various products used for cloud and dust detection on the 17th June, 2020 at 19:12  
 UTC. Fig. 3(a) illustrates the SEVIRI dust RGB composite, based on three thermal bands (8.7, 10.8 and 12  $\mu$ m) from SEVIRI  
 such that shades of pink to violet are interpreted as dust. Fig. 3(b) represents the corresponding SEVIRI cloud mask (CLM)

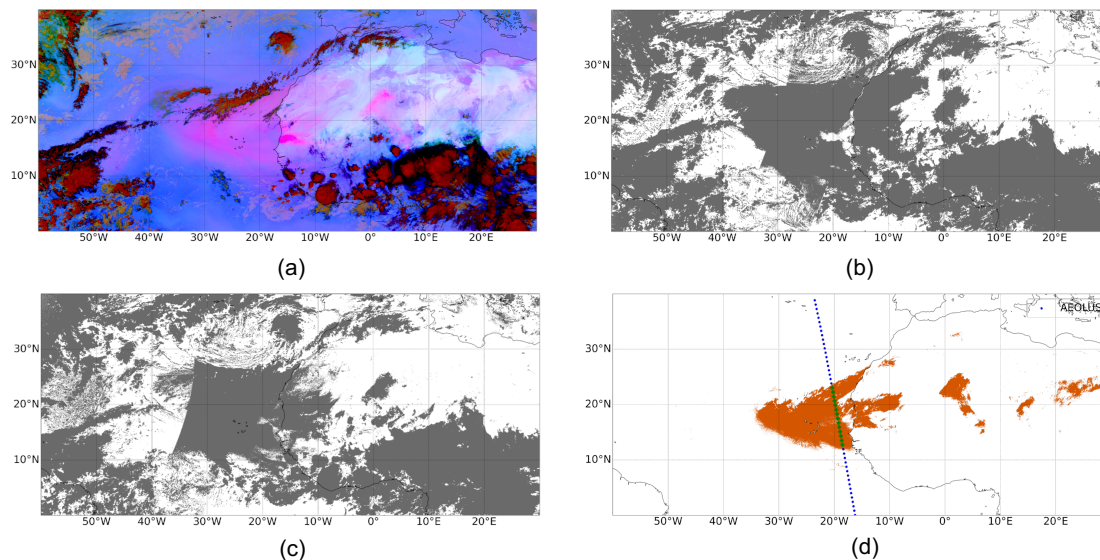


**Figure 3.** Illustration of SEVIRI products and a generated dust flag used on the 17th June 2020 at 19:12 UTC. (a) SEVIRI dust RGB composite, where shades of pink to violet denote dust. (b) SEVIRI CLM cloud mask, highlighting regions identified as clouds in grey. (c) CM SAF cloud mask, showing an alternative cloud identification product by EUMETSAT Satellite Application Facility on Climate Monitoring. (d) Generated dust flag using the method proposed by Ashpole and Washington (2012), illustrating the accurate automatic detection of dust regions over the entire study area. The blue dots in (d) represent the footprint of Aeolus at a horizontal step of approximately 87 km, and the green plus sign marks the location where Aeolus detects dust aerosol in that profile.

195 product<sup>1</sup>, while Fig. 3(c) shows the SEVIRI cloud mask generated by the EUMETSAT Satellite Application Facility on Climate  
Monitoring (CM SAF)<sup>2</sup>. A comparison of these masks reveals that the CM SAF product has fewer regions misclassified as  
cloud compared to the CLM product. A significant portion of the dust plume is still incorrectly classified as cloud in both  
products. Fig. 3(d) displays a dust mask generated using the method of Ashpole and Washington (2012), which can accurately  
200 identify dust regions over the entire area automatically. The SEVIRI instrument completes a full-disk scan every 15 minutes,  
ensuring a SEVIRI dust flag is available within 7.5 minutes of each ALADIN observation. While ALADIN observations have  
a horizontal resolution of  $\sim 87$  km, the SEVIRI sub-satellite points offer a resolution of  $\sim 3$  km. In this study, each geolocation  
is resampled at a 3 km resolution along the satellite track, and a profile is designated as a dust aerosol observation if 95% of  
the corresponding resampled footprints are flagged as dust in the relevant SEVIRI data.

<sup>1</sup><https://navigator.eumetsat.int/product/EO:EUM:DAT:MSG:CLM>

<sup>2</sup>[https://navigator.eumetsat.int/product/EO:EUM:CM:MSG:CMA\\_SEVIRI\\_V001](https://navigator.eumetsat.int/product/EO:EUM:CM:MSG:CMA_SEVIRI_V001)





#### 4 Case study - June 2020 Saharan dust

205 In June 2020, a large-scale uplift and subsequent transport of dust from the Sahara to the Americas was observed. This event represented the highest AOD for the month of June since 2002. Characterised by continuous emissions over four days, the dust was elevated to altitudes above 6 km due to strong updrafts. The African Easterly Jet facilitated rapid westward long-range transport of the dust (Francis et al., 2020). This study evaluates the accuracy of two space-borne lidar instruments in quantifying this substantial dust event.

210 Evaluating the accuracy in dust aerosol retrievals between CALIOP and ALADIN is not straightforward. This complexity is largely due to the fact that CALIOP measures the total atmospheric backscattered signals, while ALADIN is designed to only measure the co-polar part of these signals. When non-spherical particles such as dust, volcanic ash, and ice crystals are probed, it can lead to ALADIN underestimating the backscatter coefficients. This was illustrated during the Polly<sup>XT</sup> ground lidar experiments conducted in the eastern Mediterranean on the 10<sup>th</sup> July 2019, showing ALADIN can underestimate the  
215 aerosol backscatter coefficients by up to 33% when non-spherical mineral particles are recorded (Gkikas et al., 2023).

To address this issue, the method of Abril-Gago et al. (2022) was used to convert between the co-polar part and total particle backscatter coefficient. The formula used to convert between the 355 nm co-polar part and total backscatter coefficient is

$$\beta_{\text{co},355}^{\text{part}} = \frac{\beta_{\text{total},355}^{\text{part}}}{1 + \delta_{\text{circ},355}^{\text{part}}} \quad (1)$$

where  $\beta_{\text{co},355}^{\text{part}}$  is the ALADIN 355 nm co-polar part of the particle backscatter coefficient, and  $\beta_{\text{total},355}^{\text{part}}$  is the 355 nm total  
220 backscatter coefficient. The circular particle depolarization ratio at 355 nm,  $\delta_{\text{circ},355}^{\text{part}}$ , is typically not directly measured. It can be estimated if the linear particle depolarization ratio is measured (Mishchenko and Hovenier, 1995), using

$$\delta_{\text{circ},355}^{\text{part}} = \frac{2\delta_{\text{linear},355}^{\text{part}}}{1 - \delta_{\text{linear},355}^{\text{part}}} \quad (2)$$

where  $\delta_{\text{linear},355}^{\text{part}}$  is the linear particle depolarization ratio at 355 nm. ALADIN does not measure the linear particle depolarization ratio, and CALIOP only measures the linear particle depolarization ratio at 532 nm. To address this, a further conversion is  
225 required:

$$\delta_{\text{linear},355}^{\text{part}} = K_{\delta} \cdot \delta_{\text{linear},532}^{\text{part}} \quad (3)$$

where  $K_{\delta}$  is the spectral conversion factor. Abril-Gago et al. (2022) collected a dataset consisting of measures for  $\delta_{\text{linear},355}^{\text{part}}$   
and  $\delta_{\text{linear},532}^{\text{part}}$  for various aerosol types from the literature, and applied a linear regression to estimate the spectral conversion factor  $K_{\delta}$ . For dust, the best linear fit was found to be  $K_{\delta} = 0.82 \pm 0.02$ . This value is used in this study for evaluating the  
230 backscatter coefficients obtained from CALIOP and ALADIN.

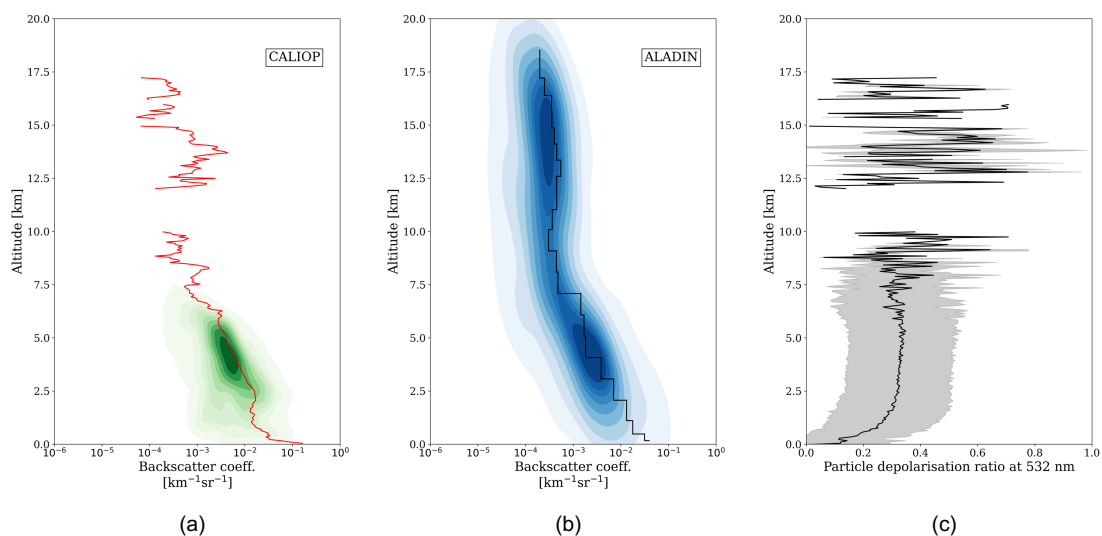


**Figure 4.** Comparison of aerosol backscatter coefficients between CALIOP and ALADIN for the Saharan dust event spanning 14<sup>th</sup> to 24<sup>th</sup> June 2020. The analysis covers the region between 60° W and 30° E in longitude and 0° and 40° N in latitude. (a) The green gradient represents the density distribution of particle backscatter coefficients derived from all available CALIOP profiles over the 11-day period, while the red curve indicates the average backscatter coefficient profile at 532 nm. (b) The blue gradient depicts the density distribution of particle backscatter coefficients from all available ALADIN profiles over the same period, with the black curve representing the average backscatter coefficient profile at 355 nm. (c) This panel illustrates the depolarization ratio at 532 nm from CALIOP measurements, where the black curve signifies the mean, and the grey shadow denotes the standard deviation.

Figure 4 illustrates the aerosol backscatter coefficients derived from CALIOP and ALADIN during the 11-day Saharan dust event that began on 14<sup>th</sup> June 2020. The green and blue gradients in each subplot represent the density distribution of dust backscatter coefficients, retrieved at 532 nm for CALIOP and 355 nm for ALADIN, respectively. The respective solid lines depict the mean backscatter coefficients calculated from all retrievals throughout the observed period. For the sake of  
235 comparison, the ALADIN aerosol retrievals in Fig. 4 (a) have been converted from co-polar to total backscatter coefficients, aligning them with the CALIOP aerosol retrievals in Fig. 4 (b). The conversion process involved acquiring  $\delta_{\text{linear},532}^{\text{part}}$  from the CALIOP measurements depicted in Fig. 4 (c). Between altitudes of 2.5 and 7 km, the depolarization ratio remains fairly constant with a mean value of 0.32. This depolarization ratio aligns with results obtained from other experiments conducted on Saharan dust (Liu et al., 2008), which reported a mean depolarization ratio of 0.32 at the upper part of the dust layer. The  
240 observed decrease in the depolarization ratio in the lower part below 2.5 km is attributed to the mixing of spherical maritime aerosols, known for generally having lower depolarization ratios.

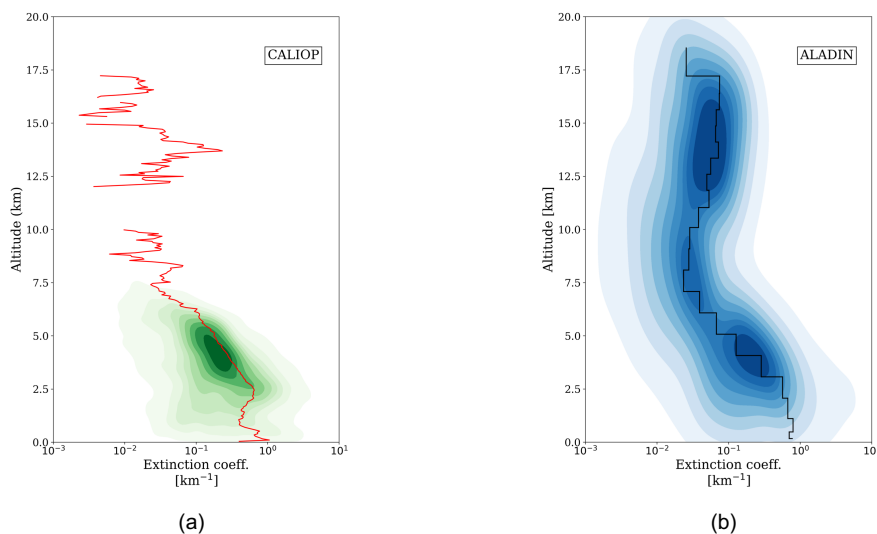


**Figure 5.** Comparison of aerosol backscatter coefficients between CALIOP (a) and ALADIN (b) for the Saharan dust event spanning 14<sup>th</sup> to 24<sup>th</sup> June 2020.

In general, CALIOP and ALADIN show good consistency in detecting dust aerosols, with evidence of dust being uplifted to 7 km. Disparities between CALIOP and ALADIN backscatter coefficients can be primarily traced back to four factors: 1) the spectral difference between 532 and 355 nm; 2) the timing discrepancy as the two instruments are scanning different segments  
245 of the dust plume at different times of the day; 3) ALADIN's coarser sampling rate compared to CALIOP, on both the vertical and horizontal scales, which may cause ALADIN to underestimate aerosol backscatter coefficients at bins with lower aerosol mixing ratios; 4) the conversion from ALADIN's co-polar to total backscatter coefficients involves the use of  $K_{\delta}$ , an empirical value of 0.82 obtained from linear fitting for dust aerosols, which could introduce bias during the conversion process. A noteworthy observation from Fig. 4 is the lack of aerosol detection above 8 km by CALIOP, contrasted with ALADIN's ability  
250 to provide an equivalent quantity of aerosol retrievals as the lower atmosphere. This divergence fundamentally originates from the distinct retrieval approaches employed by these two systems. While CALIOP's retrieval relies on an initial aerosol type identification, this constraint is non-existent in ALADIN's retrieval approach. This discrepancy reflects similar issues addressed by Kim et al. (2017), which investigated the bias within CALIOP's column AOD due to undetected aerosol layers. This study focuses on the investigation of aerosol retrievals concentrated within dust layers. Assessing the accuracy of ALADIN's aerosol  
255 retrievals within the upper atmospheric region exceeding the dust layer is beyond the scope of this work. A comprehensive evaluation of whether ALADIN outperforms CALIOP in the detection of weak aerosol signals necessitates an analysis of global aerosol retrievals, including a wide range of aerosol types and distributions. The investigation of this topic will be the subject of future research efforts.

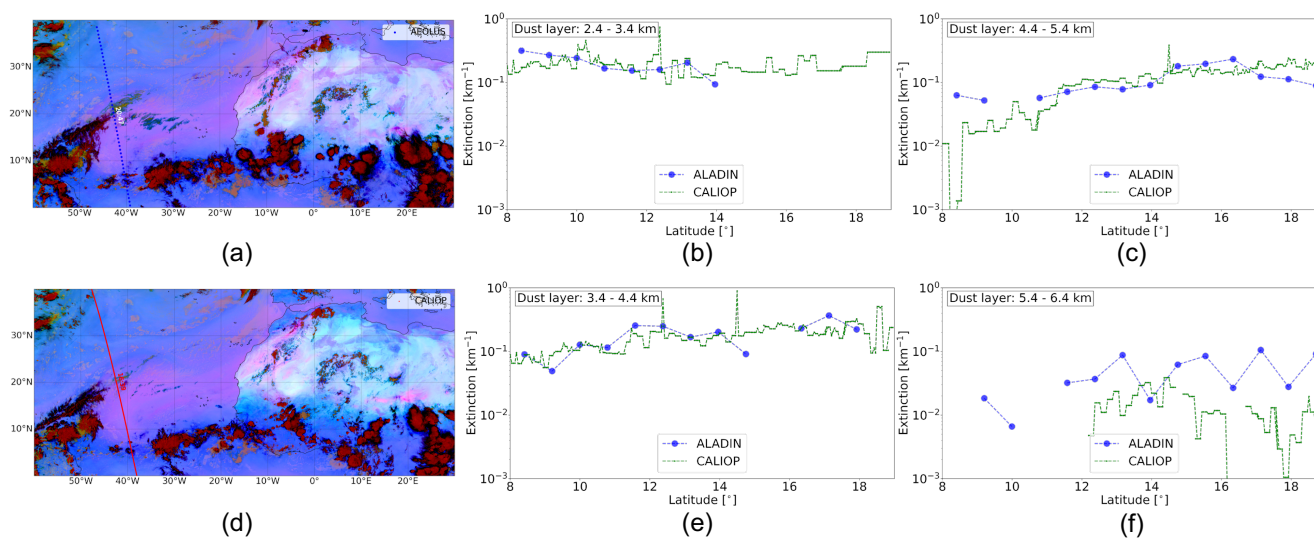


Figure 5 presents a comparison of aerosol extinction coefficients as measured by CALIOP and ALADIN, derived from  
260 the same experimental conditions described in Fig. 4. Although the two instruments generally show a good agreement in  
their measurement of extinction coefficients within the dust layer, minor disparities are also apparent. Apart from the spectral  
difference, time discrepancy, and contrasting sampling rates, this divergence is largely attributed to the differences inherent in  
the extinction retrieval methods of the two instruments. CALIOP's extinction retrieval relies on a predefined lidar ratio tailored  
for specific aerosol types. In contrast, ALADIN's backscatter and extinction coefficient retrievals operate independently of  
265 each other. The estimation of the lidar ratio for a given aerosol event can introduce its own set of biases. These biases could be  
further magnified in scenarios where the aerosol mixture deviates from the prescribed types. For instance, in this case study,  
the lidar ratio in the lower atmosphere below 2.5 km is influenced by both dust and maritime aerosols, leading to an augmented  
bias in the lidar ratio estimation.

## 5 Experiments over collocated orbits

270 Figure 6 displays a pair of collocated orbits, specifically between 50° W and 40° W, on the 24<sup>th</sup> of June 2020. The overpasses for  
Aeolus and CALIPSO are represented in Fig. 6(a) at 20:47 UTC and in Fig. 6(d) at 16:39 UTC, respectively. The background,  
as captured by the corresponding SEVIRI dust RGB images, illustrates the relative stability of the dust plume during this  
4-hour period. Additionally, this overpass spans a considerable distance across the dust plume that is free of clouds. Fig. 6(b),  
(e), (c), and (f) respectively present the extinction coefficients of the dust layer at various altitudes: 2.4 - 3.4 km, 3.4 - 4.4 km,  
275 4.4 - 5.4 km, and 5.4 - 6.4 km. These layers have been determined based on the ALADIN grid. Collocated CALIOP retrievals  
were upscaled from a resolution of 0.03 km to match this resolution. Layers beneath 2.4 km are not shown due to the reduction  
in accuracy from ALADIN resulting from low signal-to-noise ratios. ALADIN and CALIOP extinction retrievals demonstrate  
qualitatively good agreement. For Fig. 6(b), both measurements show an extinction of  $\sim 0.15 \text{ km}^{-1}$ , except where ALADIN  
observations fail quality-control. This is a common occurrence for the bottom layer of a thick aerosol layer, where signals are  
280 heavily attenuated by the overlying layers. For the middle layers of the dust, ALADIN and CALIOP extinction values display  
good agreement in both magnitude and structure. At the top layer between 5.4 - 6.4 km, a very thin dust layer is detected by  
both measurements. However, ALADIN exhibits larger values of extinction coefficient, possibly resulting from the temporal  
and spatial variability in the measurements. In this instance for the specific lidar overpass, there were no coinciding third-party  
aerosol observations available.

285 Another example of retrieval comparison is illustrated in Fig. 7, featuring descending orbits with CALIPSO overpassing at  
04:16 UTC on the 19<sup>th</sup> of June 2020, and Aeolus overpassing four hours later. This comparison primarily focuses on retrievals  
at the peak of this dust event, which is characterised by high AOD values. The extinction retrievals across the upper two  
layers (Fig. 7(c,f)), exhibit a consistent level of agreement, reflecting patterns previously observed in Fig. 6. This example also  
underscores the divergences in the extinction retrievals from the two instruments within high AOD regions, which become more  
290 pronounced within the middle and bottom layers. In Fig. 7(e), ALADIN retrievals depict a drop within the regions between 14°  
N and 20° N. Similarly, for the bottom layer (Fig. 7(b)), ALADIN observations fail to provide quality-controlled retrievals for



**Figure 6.** Comparison of aerosol extinction retrievals from collocated orbits on the 24<sup>th</sup> June 2020, featuring (a) an Aeolus overpass at 20:47 and (d) a CALIPSO overpass at 16:39, with SEVIRI dust RGB displayed in the background of each. The extinction retrievals from cloud-free regions located between 8° N and 19° N are compared across various altitude layers: (b) 2.4 - 3.4 km, (e) 3.4 - 4.4 km, (c) 4.4 - 5.4 km, and (f) 5.4 - 6.4 km.

an extended area beginning from 10° N and continuing onwards. This example illuminates a common problem with ALADIN extinction retrieval: retrievals at the base of a thick aerosol layer are very likely to be significantly underestimated or excluded by quality control due to low SNRs. A further intriguing insight arises from the layer between 3.4 - 4.4 km (Fig. 7(e)). By  
 295 filtering out retrievals between 14° N and 20° N, it becomes clear that both instruments efficiently track the spatial evolution of the dust, showing reasonable alignment. This agreement experiences a slight deviation owing to the projection of two datasets with minor geolocation differences onto a linear latitude-based scale. A noteworthy observation is that ALADIN persistently records an extinction coefficient higher by  $\sim 0.2$  compared to CALIOP. This discrepancy in absolute extinction coefficients between ALADIN and CALIOP only becomes discernible under two specific conditions: 1) when the extinction within the  
 300 layer is high - as otherwise the absolute difference substantially decreases, and 2) when the SNR for ALADIN is sufficiently high to surpass the threshold. The hypothesis to explain this phenomenon is that ALADIN, under this given aerosol condition, has higher lidar ratios than CALIOP. A higher lidar ratio inherently leads to elevated extinction coefficients. In light of this, the subsequent section investigate this discrepancy.

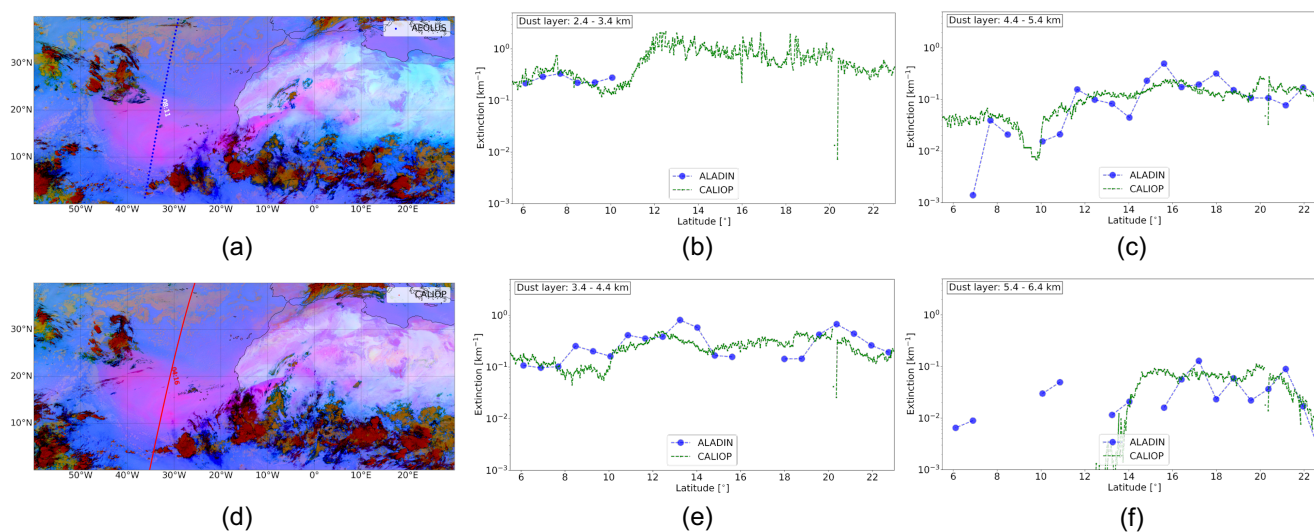


**Figure 7.** Comparison of aerosol extinction retrievals from collocated orbits on the 19<sup>th</sup> June 2020, featuring (a) an Aeolus overpass at 08:11 and (d) a CALIPSO overpass at 04:16. For details on the background display and altitude layers compared, refer to Fig. 6.

## 6 Lidar ratio and extinction retrievals

305 Figure 8 presents one of the rare instances where both collocated CALIOP profiles and cloud-free MODIS Aqua AOD measurements are available during this dust event. Fig. 8(a) shows the MODIS Aqua AOD at a 3-km resolution, together with the CALIPSO orbit track, while Fig. 8(b) depicts the corresponding CALIOP vertical feature mask. The CALIOP vertical feature mask highlights the dust plume in orange, but it also includes profiles exhibiting fully attenuated bins, represented as black at lower altitudes. To calculate the column AOD from CALIOP extinction retrievals, it is essential to exclude these profiles with  
 310 fully attenuated bins.

Figure 9 compares AOD between MODIS Aqua and CALIOP for the scene depicted in Fig. 8(a). Each CALIOP profile is paired with the nearest valid, cloud-free MODIS Aqua AOD observations. Within the latitude range of 12° N to 20° N, it is evident that the CALIOP column AOD is considerably underestimated when compared with MODIS Aqua data. Given that CALIOP retrievals have already excluded vertical profiles containing fully attenuated bins, this AOD underestimation cannot  
 315 be attributed to lost retrievals from the dust's bottom layer.

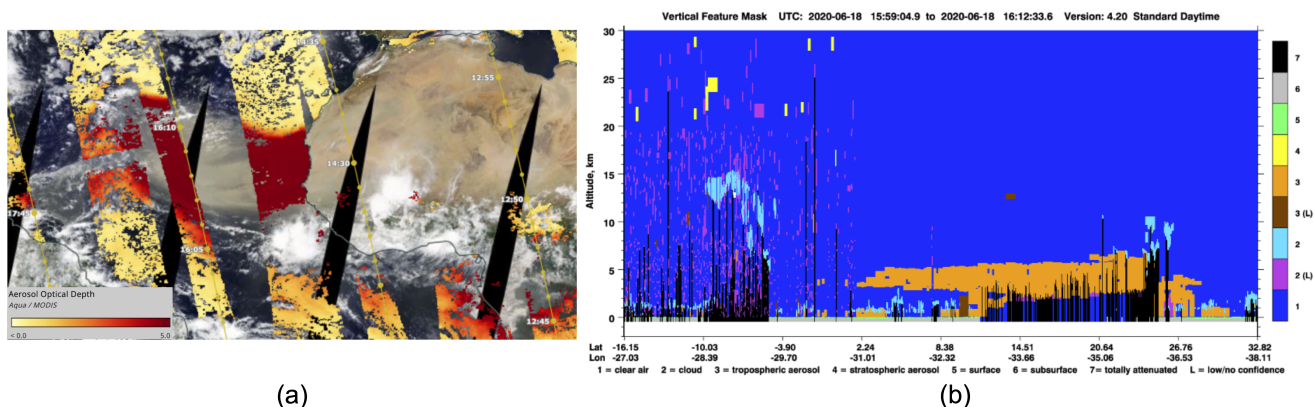


**Figure 8.** Collocated MODIS Aqua and CALIPSO observations at 16:10 UTC on the 18<sup>th</sup> of June 2020. Panel (a) displays the MODIS Aqua cloud-free AOD accompanied by the ascending CALIPSO track (available from NASA Worldview, last accessed on the 3<sup>rd</sup> of July 2023). Panel (b) illustrates the corresponding CALIOP vertical feature mask.

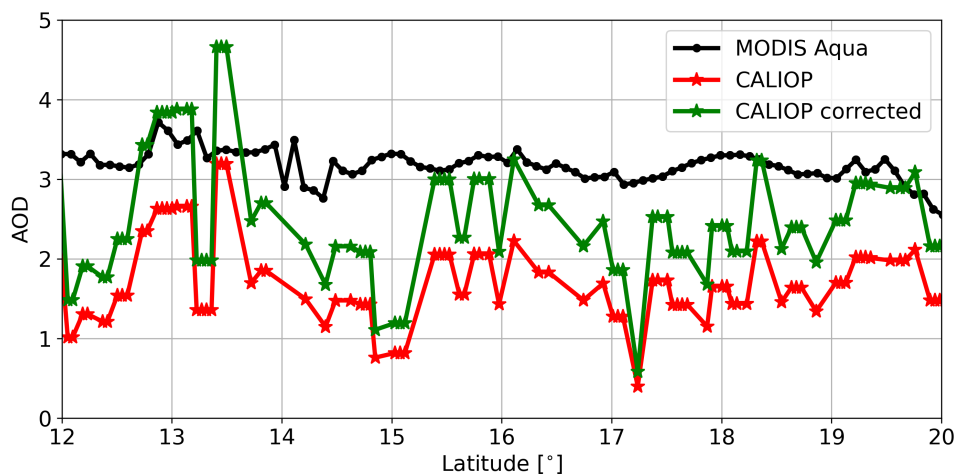


**Figure 9.** Contrast between MODIS Aqua and CALIOP AOD, derived from observational data illustrated in Fig. 8(a). MODIS Aqua AOD is selected exclusively from cloud-free retrievals. The CALIOP AODs have excluded profiles containing fully attenuated bins at any altitudes. The original and corrected CALIOP AODs are shown in red and green, respectively.

In Version 3 and previous releases, a lidar ratio of 40 sr at 532 nm was adopted for CALIOP dust retrievals. Several studies suggest that a larger lidar ratio may be appropriate (Schuster et al., 2012; Papagiannopoulos et al., 2016; Wandinger et al., 2010). With the most recent Version 4 retrieval scheme, CALIOP has increased the lidar ratio of dust to 44 sr for 532 nm (Kim et al., 2018). Dust lidar ratios demonstrate significant regional variability, ranging between 35 and 60 sr (Mamouri et al.,

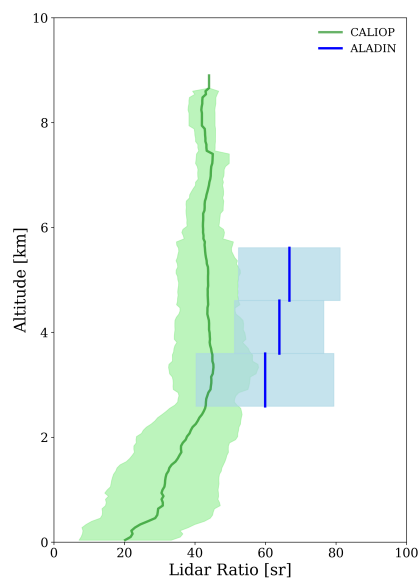


**Figure 10.** Lidar ratios derived for the dust event from 18<sup>th</sup> - 19<sup>th</sup> June 2020 with CALIOP depicted in green and ALADIN in blue. The computation of ALADIN lidar ratios incorporated the conversion from co-polar to total backscatter signals.

320 2013; Nisantzi et al., 2015). Implementing a globally adaptable lidar ratio to accommodate various dust types is complicated, as it requires identifying the source region of the transported dust. Lidar ratios can be extracted from ALADIN observations. However, the derived lidar ratios are frequently noisy and can possess exceptionally small or large values, as the retrieval process is not constrained by the lidar ratios. During the analysis of lidar ratios from ALADIN aerosol retrievals, these noisy values should be filtered out.

325 Figure 10 presents the lidar ratio calculated between the 18<sup>th</sup> and 19<sup>th</sup> of June 2020 for all valid CALIOP and ALADIN retrievals. CALIOP retrievals use an average lidar ratio of 43.5 sr above 2.5 km — an area less impacted by maritime aerosols and regarded as the dust layer. For ALADIN retrievals, a selective filtering strategy has been implemented, maintaining only data within the 2.4 to 5.8 km altitude range that best characterises the dust layers. Within this particular altitude segment, the mean lidar ratio for dust layers stands at 63.5 sr. Although no established physical equations convert lidar ratios between 355  
330 nm and 532 nm, multiple experiments with ground-based Raman lidars and airborne HSRLs have demonstrated no wavelength dependence of dust lidar ratios at these wavelengths, as detailed in Table 1.

Based on the information supplied in Table 1, it is assumed that  $LR_{355\text{ nm}}/LR_{532\text{ nm}} = 1$ , thereby justifying the selection of a lidar ratio of 63.5 sr for the correction of CALIOP extinction retrievals at 532 nm. The extinction coefficient  $\alpha_{532(\text{corr})}$  is then corrected by multiplying it with  $LR_{\text{updated}}/LR_{\text{CALIOP}}$ , where  $LR_{\text{updated}}$  is set to 63.5 sr and  $LR_{\text{CALIOP}}$  is derived from CALIOP





	lidar Ratio (lr)		
	LR <sub>355 nm</sub>	LR <sub>532 nm</sub>	LR <sub>355 nm</sub> / LR <sub>532 nm</sub>
Feb 2021 (Haarig et al., 2022)	47 sr	50 sr	0.94
Mar 2021 (Haarig et al., 2022)	49 sr	46 sr	1.07
Jan 2008 (Groß et al., 2011)	63 sr	63 sr	1.0
May 2006 (Tesche et al., 2009)	55 sr	56 sr	0.98

**Table 1.** Lidar ratios at 355 and 532 nm derived by various previous studies.

335 output values. This scaling method is an approximation, as a different lidar ratio can alter the lidar profile and subsequently affect the retrieval process.

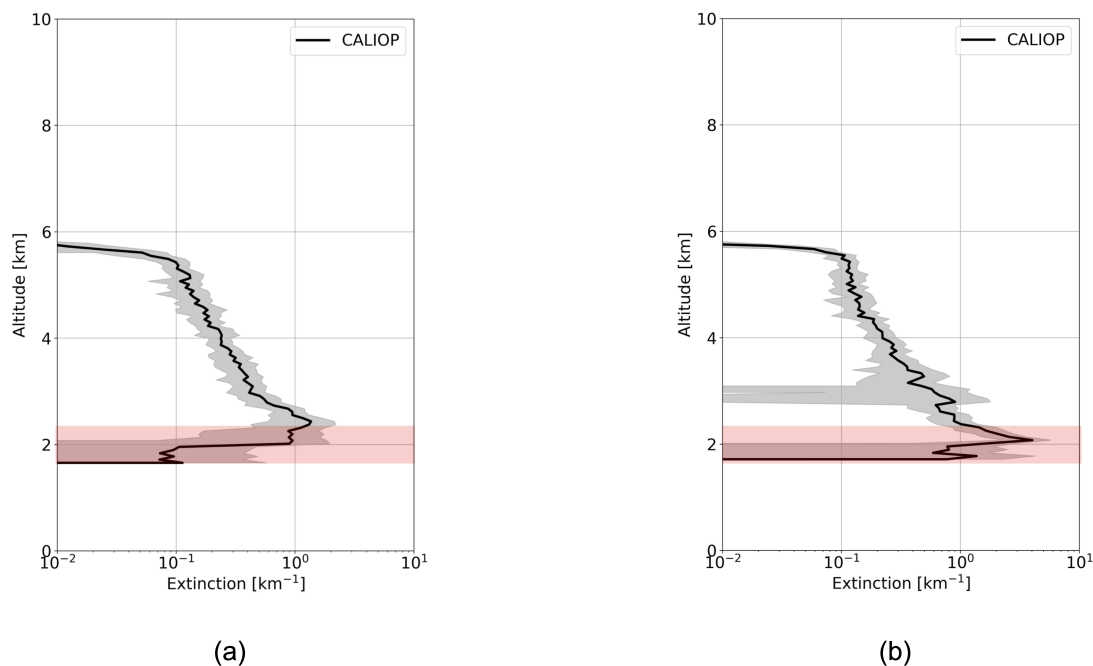
Figure 9 displays the revised CALIOP AOD values, represented in green, which are obtained through the correction of extinction retrievals. By applying a correction factor of  $LR_{ALADIN}/LR_{CALIOP}$ , the extinction and AOD values increase by 46%. This augmentation is proportionally applied to both extinction and AOD, thereby measurements exhibiting larger AOD values witness a more significant increase during the correction, and vice versa. As depicted in Fig. 9, following the correction, a subset of CALIOP AOD values better align with the MODIS AOD. However, there remain certain CALIOP values are significantly lower than the MODIS AOD values.

Fig. 11 shows the vertical distribution of extinction profiles for all CALIOP measurements in Fig. 9 classified into two groups. The first group consists of extinction profiles with a AOD below 1.8, illustrated in Fig. 11 (a), which includes 35 CALIOP profiles. The second group includes extinction profiles with a AOD exceeding 1.8, demonstrated in Fig. 11 (b), containing 24 CALIOP profiles. Both groups capture dust aerosols starting from 1.65 km and dissipating at 5.85 km. The two sets of extinction profiles exhibit a strong similarity in terms of extinction magnitude above 2.4 km. Below 2.4 km, as marked by the red shaded area, the two groups of extinction profiles present considerable discrepancies.

	Dust layer AOD	
	layer between 0 and 2.4 km	layer between 2.4 and 7 km
Total column AOD < 1.8	0.413 ± 0.443	1.015 ± 0.365
Total column AOD > 1.8	1.094 ± 0.884	1.021 ± 0.542

**Table 2.** Dust layer AOD for various CALIOP measurements as depicted in Fig. 11.

Table 2 gives the layer AOD values for both groups of CALIOP extinction profiles, those exhibiting higher (> 1.8) and lower (< 1.8) column AOD measurements. Within the dust layer between 2.4 and 7 km, both groups of measurements present similar layer AODs, 1.021 and 1.015 respectively. Pertaining to the dust layer below 2.4 km, CALIOP measurements begin to reveal the inherent limitation of lidar measurements – the potential for strong attenuation beneath dense aerosol/cloud layers. CALIOP measurements with a column AOD below 1.8 encapsulate those profiles that still feature strongly attenuated bins at the base of the dust layer, despite the implementation of the described filtering strategy. The grouped extinction profile indicate



**Figure 11.** Averaged CALIOP extinction profiles corresponding to the measurements illustrated in Fig. 9. (a) The average extinction profile for the 35 profiles with a column AOD less than 1.8. (b) The average extinction profile for the 24 profiles with a column AOD exceeding 1.8. Grey shaded areas denotes the standard deviation of extinction. Red highlights areas where notable discrepancies are observed between the two groups of extinction measurements.

355 a mean layer AOD of 0.413 between the 0 and 2.4 km layer, accompanied by a considerable standard deviation due to the random distribution of strongly attenuated bins along the satellite track. Conversely, the alternative set of measurements devoid of strongly attenuated bins demonstrates a layer AOD of 1.015 between 0 and 2.4 km. These extinction profiles align well with the MODIS column AOD following the correction of extinction values using the ALADIN lidar ratio.

## 7 Vertical transport of dust aerosol

360 CALIOP, operating as a near-nadir viewing instrument with a narrow cross-track coverage, suffers from limited temporal resolution, with a revisit time of  $\sim 16$  days. This limitation constrains CALIOP's capacity to track the localised vertical transport of plumes - such as ash, dust, and smoke - which are frequently linked with extensive horizontal transportation spanning several days to tens of days. Development and preparation for the launch of additional spaceborne atmospheric lidars continues. For instance, EarthCARE is scheduled for launch in 2024, with Aeolus-2 expected to follow near the end of the decade. The  
365 growing presence of atmospheric lidars in space is expected to enhance synergies among different lidars. This would potentially increase the quantity of available observations of aerosol vertical distribution, improving the ability to track the vertical

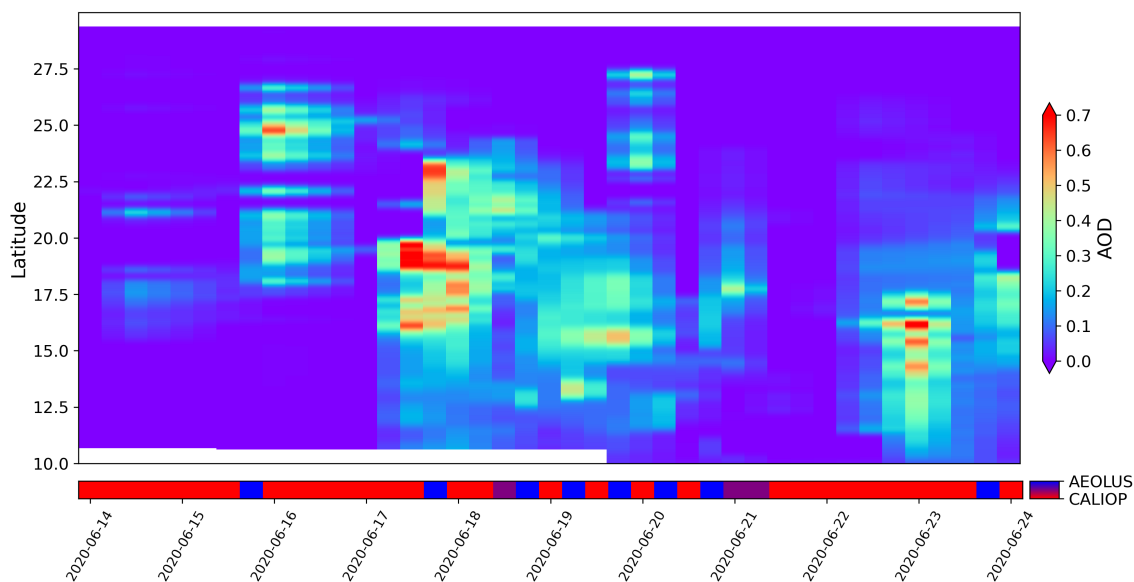


**Figure 12.** Illustration of the synergy between CALIOP and ALADIN layer AOD within the 4.5 - 6.5 km altitude range, between [40° W, 20° W], covering the 14<sup>th</sup> to the 20<sup>th</sup> of June 2020. This vertical layer includes 2 ALADIN bins and 33 CALIOP bins. The lower red-blue colourbar denotes the contributions from the two distinct lidars, with blue signifying ALADIN, red representing CALIOP, and purple indicating both. Both measurements have undergone cloud screening to ensure that this figure solely represents the evolution of dust aerosols within this layer.

transport of aerosols across various locales. Fig. 12 presents a proof-of-concept illustrating the synergy between CALIOP and ALADIN in tracking the dust plume that penetrated the altitude layer between 4.5 and 6.5 km.

As depicted in Fig. 12, the two satellites align well in detecting the dust aerosols that ascended to a height of 4.5 - 6.5 km on the 16<sup>th</sup> and 17<sup>th</sup> in the area of interest. The peak was noted by the end of the 17<sup>th</sup>, when the layer AOD surpassed 0.7. The dust aerosols remained confined within this region, and were continuously observed by the two satellites over the subsequent 5 days. This observation is consistent with the findings in Dai et al. (2022), which used reanalysis data from ECMWF and trajectory data from HYSPLIT to affirm that the dust plumes were transported within the northeasterly trade-wind zone between latitudes of 5° N and 30° N and altitudes of 0 and 6 km.

## 375 8 Conclusions

In 2018, the first spaceborne HSRL ALADIN was launched onboard the Aeolus satellite. This study undertakes an assessment of ALADIN's performance in retrieving the aerosol backscatter coefficient, extinction coefficient and lidar ratio using its Level-2 SCAMB products. The aerosol retrievals between ALADIN and CALIOP were compared during the massive Saharan



dust event of June 2020. This is the most intense dust event of the past two decades, lofting dust particles to over 6 km and  
380 transporting dust all the way to the Americas.

The ALADIN does not possess the capability to measure the particle depolarization ratio, constraining its ability to dis-  
criminate between aerosols and clouds. This study integrates measurements from the SEVIRI instrument, onboard the MSG  
geostationary satellite, as a dust feature mask. This operational feature ensures that a SEVIRI dust flag is available for every  
ALADIN observation, with a maximum temporal discrepancy of 7.5 minutes. This mask allows a more precise evaluation of  
385 ALADIN's observations by isolating data predominantly influenced by dust aerosols despite the low spatial resolution.

ALADIN only detects the co-polar component of backscattered signals, potentially leading to an underestimation of the  
backscatter coefficient. During the June 2020 Saharan dust case study, the co-polar component of the aerosol backscatter co-  
efficient was converted to represent the total backscatter coefficient. An average taken between 14<sup>th</sup> - 24<sup>th</sup> June 2020 reveals  
a good agreement in backscatter and extinction coefficients from ALADIN and CALIOP, with both instruments showing dust  
390 ascending to 7 km. Discrepancies still persist between the two satellites' retrieval. These discrepancies can be attributed to: 1)  
The spectral difference, with ALADIN retrieval operating at 355 nm and CALIOP at 532 nm. 2) The different overpass timings  
of the satellites. 3) The horizontal sampling distance: ALADIN covers 87 km, whereas CALIOP spans 5 km. 4) Uncertainties  
arising during the conversion from ALADIN's co-polar component to the total backscatter coefficient. When comparing ex-  
tinction coefficients, an extra contributor to the discrepancy is the lidar ratio. While CALIOP assigned a predefined lidar ratio  
395 for dust, ALADIN's extinction retrieval operates independently of the lidar ratio.

A detailed analysis was conducted to compare the extinction coefficients obtained from collocated ALADIN and CALIOP  
orbits across various altitude layers. To align with ALADIN's observations, CALIOP's higher vertical resolution data were  
aggregated into these 1 km layers. Generally, the quality-controlled ALADIN and CALIOP extinction retrievals converge well  
within the middle and top of the dust layer. However, in the bottom layer ranging from 2.4 to 3.4 km, ALADIN's extinction  
400 retrievals are strongly affected by diminished SNRs.

During this dust event, only one collocated orbit between CALIOP and MODIS was available for a comprehensive AOD  
comparison. For accuracy, this comparison intentionally omitted CALIOP profiles containing fully attenuated bins from the  
dust layer's base. Nonetheless, the findings reveal that CALIOP's column AOD is significantly lower than that observed by  
MODIS Aqua AOD. The lidar ratio is a key parameter in extinction retrievals, with potential to introduce biases that could lead  
405 to disparities in overall AOD calculations. The lidar ratios of dust aerosols were investigated based on observations between  
18<sup>th</sup> and 19<sup>th</sup> June 2020. CALIOP used a lidar ratio averaging at 43.5 sr. The lidar ratios derived from ALADIN observations  
showed large variability. Following rigorous filtering, the ALADIN dataset produced a mean lidar ratio of 63.5 sr for the same  
region and interval.

By applying the ALADIN lidar ratio as a correction for the CALIOP extinction retrievals, the CALIOP-derived AOD re-  
410 trievals increased by 46%, resulting in a closer alignment of a substantial portion of the corrected CALIOP AOD with MODIS  
AOD. Nonetheless, certain CALIOP profiles continue to reflect AOD values that are significantly lower than those from  
MODIS. Separating these profiles based on the MODIS AOD revealed that discrepancies in overall AOD values between  
the two subsets were predominantly sourced from varying extinction retrievals beneath 2.4 km altitude. Given the dense dust



concentration in this layer, CALIOP signals are susceptible to attenuation, leading to potential anomalies in both extinction  
415 and consequent AOD calculations.

This investigation additionally offers a demonstrative application of combining ALADIN and CALIOP observations to  
derive the vertical transport of aerosols. This methodology serves as a preliminary illustration of the potential collaborative  
benefits of employing multiple spaceborne lidars to delineate aerosols' spatial trajectories. Such demonstration has significant  
implications for forthcoming spaceborne HSRL missions, including the ESA EarthCARE's ATLID lidar, set for a 2024 launch,  
420 and the anticipated Aeolus-2 set for deployment by the end of this decade.

*Author contributions.* RS, AP and RG were responsible for conceptualization and methodology. AP and RG supervised this study. RS  
performed formal analysis and visualization. RS prepared the original draft. RS, AP and RG reviewed and edited the paper. All authors  
contributed replying to reviewer's comments.

*Competing interests.* The authors declare no competing interests

425 *Acknowledgements.* This study was funded through NERC's support of the National Centre for Earth Observation, award number NE/R016518/1.  
CALIOP data obtained from the NASA Langley Research Center Atmospheric Science Data Center.. Aeolus data obtained from ESA Aeolus  
Online Dissemination Service. This work used JASMIN, the UK collaborative data analysis facility.



## References

- Abril-Gago, J., Guerrero-Rascado, J. L., Costa, M. J., Bravo-Aranda, J. A., Sicard, M., Bermejo-Pantaleón, D., Bortoli, D., Granados-  
430 Muñoz, M. J., Rodríguez-Gómez, A., Muñoz Porcar, C., Comerón, A., Ortiz-Amezcuca, P., Salgueiro, V., Jiménez-Martín, M. M., and  
Alados-Arboledas, L.: Statistical validation of Aeolus L2A particle backscatter coefficient retrievals over ACTRIS/EARLINET stations  
on the Iberian Peninsula, *Atmospheric Chemistry and Physics*, 22, 1425–1451, <https://doi.org/10.5194/acp-22-1425-2022>, 2022.
- Altaratz, O., Koren, I., Remer, L., and Hirsch, E.: Review: Cloud invigoration by aerosols—Coupling between microphysics and dynamics,  
*Atmospheric Research*, 140-141, 38–60, <https://doi.org/https://doi.org/10.1016/j.atmosres.2014.01.009>, 2014.
- 435 Amiridis, V., Wandinger, U., Marinou, E., Giannakaki, E., Tsekeri, A., Basart, S., Kazadzis, S., Gkikas, A., Taylor, M., Baldasano,  
J., and Ansmann, A.: Optimizing CALIPSO Saharan dust retrievals, *Atmospheric Chemistry and Physics*, 13, 12 089–12 106,  
<https://doi.org/10.5194/acp-13-12089-2013>, 2013.
- Ashpole, I. and Washington, R.: An automated dust detection using SEVIRI: A multiyear climatology of summertime dustiness in the central  
and western Sahara, *Journal of Geophysical Research: Atmospheres*, 117, <https://doi.org/https://doi.org/10.1029/2011JD016845>, 2012.
- 440 Baars, H., Radenz, M., Floutsi, A. A., Engelmann, R., Althausen, D., Heese, B., Ansmann, A., Flament, T., Dabas, A.,  
Trapon, D., Reitebuch, O., Bley, S., and Wandinger, U.: Californian Wildfire Smoke Over Europe: A First Example of the  
Aerosol Observing Capabilities of Aeolus Compared to Ground-Based Lidar, *Geophysical Research Letters*, 48, e2020GL092 194,  
<https://doi.org/https://doi.org/10.1029/2020GL092194>, e2020GL092194 2020GL092194, 2021.
- Bellouin, N., Quaas, J., Gryspeerdt, E., Kinne, S., Stier, P., Watson-Parris, D., Boucher, O., Carslaw, K. S., Christensen, M., Daniau, A.-  
445 L., Dufresne, J.-L., Feingold, G., Fiedler, S., Forster, P., Gettelman, A., Haywood, J. M., Lohmann, U., Malavelle, F., Mauritsen, T.,  
McCoy, D. T., Myhre, G., Mühlenthal, J., Neubauer, D., Possner, A., Rugenstein, M., Sato, Y., Schulz, M., Schwartz, S. E., Sourde-  
val, O., Storelvmo, T., Toll, V., Winker, D., and Stevens, B.: Bounding Global Aerosol Radiative Forcing of Climate Change, *Reviews  
of Geophysics*, 58, e2019RG000 660, <https://doi.org/https://doi.org/10.1029/2019RG000660>, e2019RG000660 10.1029/2019RG000660,  
2020.
- 450 Burton, S. P., Ferrare, R. A., Hostetler, C. A., Hair, J. W., Rogers, R. R., Obland, M. D., Butler, C. F., Cook, A. L., Harper, D. B., and Froyd,  
K. D.: Aerosol classification using airborne High Spectral Resolution Lidar measurements – methodology and examples, *Atmospheric  
Measurement Techniques*, 5, 73–98, <https://doi.org/10.5194/amt-5-73-2012>, 2012.
- Burton, S. P., Ferrare, R. A., Vaughan, M. A., Omar, A. H., Rogers, R. R., Hostetler, C. A., and Hair, J. W.: Aerosol classification  
from airborne HSRL and comparisons with the CALIPSO vertical feature mask, *Atmospheric Measurement Techniques*, 6, 1397–1412,  
455 <https://doi.org/10.5194/amt-6-1397-2013>, 2013.
- Dai, G., Sun, K., Wang, X., Wu, S., E, X., Liu, Q., and Liu, B.: Dust transport and advection measurement with spaceborne lidars ALADIN  
and CALIOP and model reanalysis data, *Atmospheric Chemistry and Physics*, 22, 7975–7993, <https://doi.org/10.5194/acp-22-7975-2022>,  
2022.
- Dubovik, O., Sinyuk, A., Lapyonok, T., Holben, B. N., Mishchenko, M., Yang, P., Eck, T. F., Volten, H., Muñoz, O., Veihelmann, B., van der  
460 Zande, W. J., Leon, J.-F., Sorokin, M., and Slutsker, I.: Application of spheroid models to account for aerosol particle nonsphericity in  
remote sensing of desert dust, *Journal of Geophysical Research: Atmospheres*, 111, <https://doi.org/https://doi.org/10.1029/2005JD006619>,  
2006.



- Ehlers, F., Flament, T., Dabas, A., Trapon, D., Lacour, A., Baars, H., and Straume-Lindner, A. G.: Optimization of Aeolus' aerosol optical properties by maximum-likelihood estimation, *Atmospheric Measurement Techniques*, 15, 185–203, <https://doi.org/10.5194/amt-15-185-2022>, 2022.
- 465
- Feofilov, A. G., Chepfer, H., Noël, V., Guzman, R., Gindre, C., Ma, P.-L., and Chiriaco, M.: Comparison of scattering ratio profiles retrieved from ALADIN/Aeolus and CALIOP/CALIPSO observations and preliminary estimates of cloud fraction profiles, *Atmospheric Measurement Techniques*, 15, 1055–1074, <https://doi.org/10.5194/amt-15-1055-2022>, 2022.
- Flament, T., Trapon, D., Lacour, A., Dabas, A., Ehlers, F., and Huber, D.: Aeolus L2A aerosol optical properties product: standard correct algorithm and Mie correct algorithm, *Atmospheric Measurement Techniques*, 14, 7851–7871, <https://doi.org/10.5194/amt-14-7851-2021>, 2021.
- 470
- Francis, D., Fonseca, R., Nelli, N., Cuesta, J., Weston, M., Evan, A., and Temimi, M.: The Atmospheric Drivers of the Major Saharan Dust Storm in June 2020, *Geophysical Research Letters*, 47, e2020GL090102, <https://doi.org/https://doi.org/10.1029/2020GL090102>, e2020GL090102 2020GL090102, 2020.
- 475
- Ghan, S. J., Liu, X., Easter, R. C., Zaveri, R., Rasch, P. J., Yoon, J.-H., and Eaton, B.: Toward a Minimal Representation of Aerosols in Climate Models: Comparative Decomposition of Aerosol Direct, Semidirect, and Indirect Radiative Forcing, *Journal of Climate*, 25, 6461–6476, <https://doi.org/https://doi.org/10.1175/JCLI-D-11-00650.1>, 2012.
- Gkikas, A., Gialitaki, A., Biniotoglou, I., Marinou, E., Tsihla, M., Siomos, N., Paschou, P., Kampouri, A., Voudouri, K. A., Proestakis, E., Mylonaki, M., Papanikolaou, C.-A., Michailidis, K., Baars, H., Straume, A. G., Balis, D., Papayannis, A., Parrinello, T., and Amiridis, V.: First assessment of Aeolus Standard Correct Algorithm particle backscatter coefficient retrievals in the eastern Mediterranean, *Atmospheric Measurement Techniques*, 16, 1017–1042, <https://doi.org/10.5194/amt-16-1017-2023>, 2023.
- 480
- Groß, S., Wiegner, M., Freudenthaler, V., and Toledano, C.: Lidar ratio of Saharan dust over Cape Verde Islands: Assessment and error calculation, *Journal of Geophysical Research: Atmospheres*, 116, <https://doi.org/https://doi.org/10.1029/2010JD015435>, 2011.
- Haarig, M., Ansmann, A., Engelmann, R., Baars, H., Toledano, C., Torres, B., Althausen, D., Radenz, M., and Wandinger, U.: First triple-wavelength lidar observations of depolarization and extinction-to-backscatter ratios of Saharan dust, *Atmospheric Chemistry and Physics*, 22, 355–369, <https://doi.org/10.5194/acp-22-355-2022>, 2022.
- 485
- Kim, M.-H., Omar, A. H., Vaughan, M. A., Winker, D. M., Trepte, C. R., Hu, Y., Liu, Z., and Kim, S.-W.: Quantifying the low bias of CALIPSO's column aerosol optical depth due to undetected aerosol layers, *Journal of Geophysical Research: Atmospheres*, 122, 1098–1113, <https://doi.org/https://doi.org/10.1002/2016JD025797>, 2017.
- 490
- Kim, M.-H., Omar, A. H., Tackett, J. L., Vaughan, M. A., Winker, D. M., Trepte, C. R., Hu, Y., Liu, Z., Poole, L. R., Pitts, M. C., Kar, J., and Magill, B. E.: The CALIPSO version 4 automated aerosol classification and lidar ratio selection algorithm, *Atmospheric Measurement Techniques*, 11, 6107–6135, <https://doi.org/10.5194/amt-11-6107-2018>, 2018.
- Kim, M.-H., Kim, S.-W., and Omar, A. H.: Dust Lidar Ratios Retrieved from the CALIOP Measurements Using the MODIS AOD as a Constraint, *Remote Sensing*, 12, <https://doi.org/10.3390/rs12020251>, 2020.
- 495
- Kipling, Z., Stier, P., Johnson, C. E., Mann, G. W., Bellouin, N., Bauer, S. E., Bergman, T., Chin, M., Diehl, T., Ghan, S. J., Iversen, T., Kirkevåg, A., Kokkola, H., Liu, X., Luo, G., van Noije, T., Pringle, K. J., von Salzen, K., Schulz, M., Seland, Ø., Skeie, R. B., Takemura, T., Tsigaridis, K., and Zhang, K.: What controls the vertical distribution of aerosol? Relationships between process sensitivity in HadGEM3–UKCA and inter-model variation from AeroCom Phase II, *Atmospheric Chemistry and Physics*, 16, 2221–2241, <https://doi.org/10.5194/acp-16-2221-2016>, 2016.



- 500 Koffi, B., Schulz, M., Bréon, F.-M., Griesfeller, J., Winker, D., Balkanski, Y., Bauer, S., Bernsten, T., Chin, M., Collins, W. D., Dentener, F., Diehl, T., Easter, R., Ghan, S., Ginoux, P., Gong, S., Horowitz, L. W., Iversen, T., Kirkevåg, A., Koch, D., Krol, M., Myhre, G., Stier, P., and Takemura, T.: Application of the CALIOP layer product to evaluate the vertical distribution of aerosols estimated by global models: AeroCom phase I results, *Journal of Geophysical Research: Atmospheres*, 117, <https://doi.org/https://doi.org/10.1029/2011JD016858>, 2012.
- 505 Legras, B., Duchamp, C., Sellitto, P., Podglajen, A., Carboni, E., Siddans, R., Grooß, J.-U., Khaykin, S., and Ploeger, F.: The evolution and dynamics of the Hunga Tonga–Hunga Ha’apai sulfate aerosol plume in the stratosphere, *Atmospheric Chemistry and Physics*, 22, 14957–14970, <https://doi.org/10.5194/acp-22-14957-2022>, 2022.
- Liu, Z., Omar, A., Vaughan, M., Hair, J., Kittaka, C., Hu, Y., Powell, K., Trepte, C., Winker, D., Hostetler, C., Ferrare, R., and Pierce, R.: CALIPSO lidar observations of the optical properties of Saharan dust: A case study of long-range transport, *Journal of Geophysical Research: Atmospheres*, 113, <https://doi.org/https://doi.org/10.1029/2007JD008878>, 2008.
- 510 Mamouri, R. E., Ansmann, A., Nisantzi, A., Kokkalis, P., Schwarz, A., and Hadjimitsis, D.: Low Arabian dust extinction-to-backscatter ratio, *Geophysical Research Letters*, 40, 4762–4766, <https://doi.org/https://doi.org/10.1002/grl.50898>, 2013.
- Markus, T., Neumann, T., Martino, A., Abdalati, W., Brunt, K., Csatho, B., Farrell, S., Fricker, H., Gardner, A., Harding, D., Jasinski, M., Kwok, R., Magruder, L., Lubin, D., Luthcke, S., Morison, J., Nelson, R., Neuenschwander, A., Palm, S., Popescu, S., Shum, C., Schutz, B. E., Smith, B., Yang, Y., and Zwally, J.: The Ice, Cloud, and land Elevation Satellite-2 (ICESat-2): Science requirements, concept, and implementation, *Remote Sensing of Environment*, 190, 260–273, <https://doi.org/https://doi.org/10.1016/j.rse.2016.12.029>, 2017.
- 515 McGill, M. J., Yorks, J. E., Scott, V. S., Kupchock, A. W., and Selmer, P. A.: The Cloud-Aerosol Transport System (CATS): a technology demonstration on the International Space Station, in: *Lidar Remote Sensing for Environmental Monitoring XV*, edited by Singh, U. N., vol. 9612, p. 96120A, International Society for Optics and Photonics, SPIE, <https://doi.org/10.1117/12.2190841>, 2015.
- 520 Mishchenko, M. I. and Hovenier, J. W.: Depolarization of light backscattered by randomly oriented nonspherical particles, *Opt. Lett.*, 20, 1356–1358, <https://doi.org/10.1364/OL.20.001356>, 1995.
- Mona, L., Amodeo, A., Pandolfi, M., and Pappalardo, G.: Saharan dust intrusions in the Mediterranean area: Three years of Raman lidar measurements, *Journal of Geophysical Research: Atmospheres*, 111, <https://doi.org/https://doi.org/10.1029/2005JD006569>, 2006.
- 525 Müller, D., Hostetler, C. A., Ferrare, R. A., Burton, S. P., Chemyakin, E., Kolgotin, A., Hair, J. W., Cook, A. L., Harper, D. B., Rogers, R. R., Hare, R. W., Cleckner, C. S., Obland, M. D., Tomlinson, J., Berg, L. K., and Schmid, B.: Airborne Multiwavelength High Spectral Resolution Lidar (HSRL-2) observations during TCAP 2012: vertical profiles of optical and microphysical properties of a smoke/urban haze plume over the northeastern coast of the US, *Atmospheric Measurement Techniques*, 7, 3487–3496, <https://doi.org/10.5194/amt-7-3487-2014>, 2014.
- 530 Myhre, G., Samset, B. H., Schulz, M., Balkanski, Y., Bauer, S., Bernsten, T. K., Bian, H., Bellouin, N., Chin, M., Diehl, T., Easter, R. C., Feichter, J., Ghan, S. J., Hauglustaine, D., Iversen, T., Kinne, S., Kirkevåg, A., Lamarque, J.-F., Lin, G., Liu, X., Lund, M. T., Luo, G., Ma, X., van Noije, T., Penner, J. E., Rasch, P. J., Ruiz, A., Seland, Ø., Skeie, R. B., Stier, P., Takemura, T., Tsigaridis, K., Wang, P., Wang, Z., Xu, L., Yu, H., Yu, F., Yoon, J.-H., Zhang, K., Zhang, H., and Zhou, C.: Radiative forcing of the direct aerosol effect from AeroCom Phase II simulations, *Atmospheric Chemistry and Physics*, 13, 1853–1877, <https://doi.org/10.5194/acp-13-1853-2013>, 2013.
- 535 Nisantzi, A., Mamouri, R. E., Ansmann, A., Schuster, G. L., and Hadjimitsis, D. G.: Middle East versus Saharan dust extinction-to-backscatter ratios, *Atmospheric Chemistry and Physics*, 15, 7071–7084, <https://doi.org/10.5194/acp-15-7071-2015>, 2015.
- Nowottnick, E. P., Colarco, P. R., Welton, E. J., and da Silva, A.: Use of the CALIOP vertical feature mask for evaluating global aerosol models, *Atmospheric Measurement Techniques*, 8, 3647–3669, <https://doi.org/10.5194/amt-8-3647-2015>, 2015.





- Oikawa, E., Nakajima, T., and Winker, D.: An Evaluation of the Shortwave Direct Aerosol Radiative Forcing Using CALIOP and MODIS Observations, *Journal of Geophysical Research: Atmospheres*, 123, 1211–1233, <https://doi.org/https://doi.org/10.1002/2017JD027247>, 2018.
- Omar, A. H., Winker, D. M., Vaughan, M. A., Hu, Y., Trepte, C. R., Ferrare, R. A., Lee, K.-P., Hostetler, C. A., Kittaka, C., Rogers, R. R., Kuehn, R. E., and Liu, Z.: The CALIPSO Automated Aerosol Classification and Lidar Ratio Selection Algorithm, *Journal of Atmospheric and Oceanic Technology*, 26, 1994 – 2014, <https://doi.org/https://doi.org/10.1175/2009JTECHA1231.1>, 2009.
- Papagiannopoulos, N., Mona, L., Alados-Arboledas, L., Amiridis, V., Baars, H., Biniotoglou, I., Bor-  
545 toli, D., D’Amico, G., Giunta, A., Guerrero-Rascado, J. L., Schwarz, A., Pereira, S., Spinelli, N., Wandinger, U., Wang, X., and Pappalardo, G.: CALIPSO climatological products: evaluation and suggestions from EARLINET, *Atmospheric Chemistry and Physics*, 16, 2341–2357, <https://doi.org/10.5194/acp-16-2341-2016>, 2016.
- Pappalardo, G., Amodeo, A., Apituley, A., Comeron, A., Freudenthaler, V., Linné, H., Ansmann, A., Bösenberg, J., D’Amico, G., Mattis, I.,  
550 Mona, L., Wandinger, U., Amiridis, V., Alados-Arboledas, L., Nicolae, D., and Wiegner, M.: EARLINET: towards an advanced sustainable European aerosol lidar network, *Atmospheric Measurement Techniques*, 7, 2389–2409, <https://doi.org/10.5194/amt-7-2389-2014>, 2014.
- Paschou, P., Siomos, N., Tsekeri, A., Louridas, A., Georgoussis, G., Freudenthaler, V., Biniotoglou, I., Tsaknakis, G., Tavernarakis, A., Evangelatos, C., von Bismarck, J., Kanitz, T., Meleti, C., Marinou, E., and Amiridis, V.: The eVe reference polarisation lidar system for the calibration and validation of the Aeolus L2A product, *Atmospheric Measurement Techniques*, 15, 2299–2323, <https://doi.org/10.5194/amt-15-2299-2022>, 2022.
- 555 Rogers, R. R., Vaughan, M. A., Hostetler, C. A., Burton, S. P., Ferrare, R. A., Young, S. A., Hair, J. W., Obland, M. D., Harper, D. B., Cook, A. L., and Winker, D. M.: Looking through the haze: evaluating the CALIPSO level 2 aerosol optical depth using airborne high spectral resolution lidar data, *Atmospheric Measurement Techniques*, 7, 4317–4340, <https://doi.org/10.5194/amt-7-4317-2014>, 2014.
- Schmetz, J., Pili, P., Tjemkes, S., Just, D., Kerkmann, J., Rota, S., and Ratier, A.: AN INTRODUCTION TO METEOSAT SECOND GENERATION (MSG), *Bulletin of the American Meteorological Society*, 83, 977 – 992, [https://doi.org/https://doi.org/10.1175/1520-0477\(2002\)083<0977:AITMSG>2.3.CO;2](https://doi.org/https://doi.org/10.1175/1520-0477(2002)083<0977:AITMSG>2.3.CO;2), 2002.
- 560 Schuster, G. L., Vaughan, M., MacDonnell, D., Su, W., Winker, D., Dubovik, O., Lapyonok, T., and Trepte, C.: Comparison of CALIPSO aerosol optical depth retrievals to AERONET measurements, and a climatology for the lidar ratio of dust, *Atmospheric Chemistry and Physics*, 12, 7431–7452, <https://doi.org/10.5194/acp-12-7431-2012>, 2012.
- Shipley, S. T., Tracy, D. H., Eloranta, E. W., Trauger, J. T., Sroga, J. T., Roesler, F. L., and Weinman, J. A.: High spectral resolution lidar to measure optical scattering properties of atmospheric aerosols. 1: Theory and instrumentation, *Appl. Opt.*, 22, 3716–3724, <https://doi.org/10.1364/AO.22.003716>, 1983.
- Spinhirne, J. D., Palm, S. P., Hart, W. D., Hlavka, D. L., and Welton, E. J.: Cloud and aerosol measurements from GLAS: Overview and initial results, *Geophysical Research Letters*, 32, <https://doi.org/https://doi.org/10.1029/2005GL023507>, 2005.
- Stoffelen, A., Pailleux, J., Källén, E., Vaughan, J. M., Isaksen, L., Flamant, P., Wergen, W., Andersson, E., Schyberg, H., Culoma, A.,  
570 Meynart, R., Endemann, M., and Ingmann, P.: The Atmospheric Dynamics Mission for Global Wind Field Measurement, *Bulletin of the American Meteorological Society*, 86, 73 – 88, <https://doi.org/https://doi.org/10.1175/BAMS-86-1-73>, 2005.
- Sugimoto, N., Nishizawa, T., Shimizu, A., and Jin, Y.: The Asian Dust and Aerosol Lidar Observation Network (AD-Net), in: *Light, Energy and the Environment*, p. EW2A.1, Optica Publishing Group, <https://doi.org/10.1364/EE.2016.EW2A.1>, 2016.



- Sun, K., Dai, G., Wu, S., Reitebuch, O., Baars, H., Liu, J., and Zhang, S.: Correlation between marine aerosol optical properties and wind fields over remote oceans with use of spaceborne lidar observations, *EGUsphere*, 2023, 1–34, <https://doi.org/10.5194/egusphere-2023-433>, 2023.
- Tackett, J. L., Kar, J., Vaughan, M. A., Getzewich, B. J., Kim, M.-H., Vernier, J.-P., Omar, A. H., Magill, B. E., Pitts, M. C., and Winker, D. M.: The CALIPSO version 4.5 stratospheric aerosol subtyping algorithm, *Atmospheric Measurement Techniques*, 16, 745–768, <https://doi.org/10.5194/amt-16-745-2023>, 2023.
- 580 Tesche, M., Ansmann, A., MüLLER, D., Althausen, D., Mattis, I., Heese, B., Freudenthaler, V., Wiegner, M., Esselborn, M., Pisani, G., and Knippertz, P.: Vertical profiling of Saharan dust with Raman lidars and airborne HSRL in southern Morocco during SAMUM, *Tellus B: Chemical and Physical Meteorology*, 61, 144–164, <https://doi.org/10.1111/j.1600-0889.2008.00390.x>, 2009.
- Textor, C., Schulz, M., Guibert, S., Kinne, S., Balkanski, Y., Bauer, S., Bernsten, T., Berglen, T., Boucher, O., Chin, M., Dentener, F., Diehl, T., Easter, R., Feichter, H., Fillmore, D., Ghan, S., Ginoux, P., Gong, S., Grini, A., Hendricks, J., Horowitz, L., Huang, P., Isaksen, I., Iversen, I., Kloster, S., Koch, D., Kirkevåg, A., Kristjansson, J. E., Krol, M., Lauer, A., Lamarque, J. F., Liu, X., Montanaro, V., Myhre, G., Penner, J., Pitari, G., Reddy, S., Seland, Ø., Stier, P., Takemura, T., and Tie, X.: Analysis and quantification of the diversities of aerosol life cycles within AeroCom, *Atmospheric Chemistry and Physics*, 6, 1777–1813, <https://doi.org/10.5194/acp-6-1777-2006>, 2006.
- van Zadelhoff, G.-J., Donovan, D. P., and Wang, P.: Detection of aerosol and cloud features for the EarthCARE lidar ATLID: the A-FM product, *EGUsphere*, 2023, 1–29, <https://doi.org/10.5194/egusphere-2023-145>, 2023.
- 590 Wandinger, U., Tesche, M., Seifert, P., Ansmann, A., Müller, D., and Althausen, D.: Size matters: Influence of multiple scattering on CALIPSO light-extinction profiling in desert dust, *Geophysical Research Letters*, 37, <https://doi.org/https://doi.org/10.1029/2010GL042815>, 2010.
- Wang, N., Zhang, K., Shen, X., Wang, Y., Li, J., Li, C., Mao, J., Malinka, A., Zhao, C., Russell, L. M., Guo, J., Gross, S., Liu, C., Yang, J., Chen, F., Wu, L., Chen, S., Ke, J., Xiao, D., Zhou, Y., Fang, J., and Liu, D.: Dual-field-of-view high-spectral-resolution lidar: Simultaneous profiling of aerosol and water cloud to study aerosol–cloud interaction, *Proceedings of the National Academy of Sciences*, 119, e2110756 119, <https://doi.org/10.1073/pnas.2110756119>, 2022.
- Watson-Parris, D., Schutgens, N., Winker, D., Burton, S. P., Ferrare, R. A., and Stier, P.: On the Limits of CALIOP for Constraining Modeled Free Tropospheric Aerosol, *Geophysical Research Letters*, 45, 9260–9266, <https://doi.org/https://doi.org/10.1029/2018GL078195>, 2018.
- Welton, E. J., Campbell, J. R., Spinhirne, J. D., and III, V. S. S.: Global monitoring of clouds and aerosols using a network of micropulse lidar systems, in: *Lidar Remote Sensing for Industry and Environment Monitoring*, edited by Singh, U. N., Asai, K., Ogawa, T., Singh, U. N., Itabe, T., and Sugimoto, N., vol. 4153, pp. 151 – 158, International Society for Optics and Photonics, SPIE, <https://doi.org/10.1117/12.417040>, 2001.
- Winker, D., Couch, R., and McCormick, M.: An overview of LITE: NASA’s Lidar In-space Technology Experiment, *Proceedings of the IEEE*, 84, 164–180, <https://doi.org/10.1109/5.482227>, 1996.
- 605 Winker, D. M., Pelon, J., Coakley, J. A., Ackerman, S. A., Charlson, R. J., Colarco, P. R., Flamant, P., Fu, Q., Hoff, R. M., Kittaka, C., Kubar, T. L., Treut, H. L., McCormick, M. P., Mégie, G., Poole, L., Powell, K., Trepte, C., Vaughan, M. A., and Wielicki, B. A.: The CALIPSO Mission: A Global 3D View of Aerosols and Clouds, *Bulletin of the American Meteorological Society*, 91, 1211 – 1230, <https://doi.org/https://doi.org/10.1175/2010BAMS3009.1>, 2010.
- Young, S. A., Vaughan, M. A., Garnier, A., Tackett, J. L., Lambeth, J. D., and Powell, K. A.: Extinction and optical depth retrievals for CALIPSO’s Version 4 data release, *Atmospheric Measurement Techniques*, 11, 5701–5727, <https://doi.org/10.5194/amt-11-5701-2018>, 2018.
- 610